Synthesis and Properties of Polypropylene/Multiwall Carbon Nanotube Composites

Anton A. Koval'chuk,*,† Alexander N. Shchegolikhin,‡ Vitaliy G. Shevchenko,§ Polina M. Nedorezova,† Alla N. Klyamkina,† and Alexander M. Aladyshev†

N.N. Semenov Institute of Chemical Physics of Russian Academy of Sciences, Moscow, Russia, N.M. Emanuel Institute of Biochemical Physics of Russian Academy of Sciences, Moscow, Russia, and N.S. Enikolopov Institute of Synthetic Polymer Materials of Russian Academy of Sciences, Moscow, Russia

Received February 8, 2008; In Final Form March 18, 2008; Revised Manuscript Received March 18, 2008

ABSTRACT: Isotactic polypropylene and elastomeric stereoblock polypropylene nanocomposites containing 0.1−3.5 wt % multiwall carbon nanotubes (MWCNTs) have been synthesized via the in situ polymerization approach using MAO-activated C_2- and C_1-symmetry ansa-zirconocenes, a technique that has not been previously reported in literature. Fracture morphology examination of the nanocomposites revealed very efficient distribution of the MWCNTs within the isotactic polypropylene matrix, yet interfacial adhesion level and the reinforcement efficiency were dependent on the nanotube loadings. The elastomeric stereoblock polypropylene/MWCNT and the isotactic polypropylene-based nanocomposites exhibited different morphologies depending on the synthesis peculiarities. For isotactic polypropylene, Young's modulus increased by ∼22% even at 0.1 wt % MWCNT loading, and further modulus growth was observed at higher filler contents. Relatively low permittivity values and considerable dielectric losses in microwave range infer that the obtained nanocomposites can find use as efficient electromagnetic shielding materials and microwave absorbing filters. Outstanding improvement of thermal stability (∼60 °C at maximum weight loss rate temperature) has been achieved for isotactic polypropylene upon incorporating only 3.5 wt % of carbon nanotubes.

Introduction

Since their discovery in 1991,[1] carbon nanotubes (CNTs) attract a great deal of attention owing to their unique structural and physical properties. Due to their combination of outstanding mechanical characteristics, extremely large interfacial contact area, high aspect ratio, and low mass density, CNTs are considered as the ideal reinforcement fillers for the composite materials.[2] Owing to their high flexibility, CNTs have remarkable advantage over conventional carbon fibers in processing of composites,[3] because in contrast to brittle carbon fibers that fracture easily, nanotubes usually bow without failure.[4] The combination of mechanical, electrical, and thermal transport properties of CNTs enables the obtaining of advanced multifunctional composite materials by the incorporation of nanotubes in various polymer matrices.

Isotactic polypropylene is a large-volume thermoplastic polymer of extremely high commercial importance that has numerous industrial applications including packaging, fiber manufacturing, automotive components, and construction. Modification of polypropylene performance by the CNT incorporation is a promising way of broadening the use of this material. Considerable improvement of polypropylene mechanical properties, crystallization behavior, electrical conductivity, and thermal stability can be expected based on earlier studies.[5,6] Despite the high scientific activity in synthesis and investigation of CNT-filled polymer nanocomposites, materials based on polyolefin matrices, specifically polypropylene, are rare objects of research, and most efforts are focused upon the incorporation of CNTs in polar polymers such as polyamides, PMMA, or epoxy resins. Thus, polyolefin-based nanocomposites continue to remain to insufficiently studied up to the present, and new efforts are needed in this important field.

Apart from achieving homogeneous CNT distribution in nanocomposites and preventing agglomeration of filler particles that tend to form clusters due to van der Waals attraction forces, the main challenge here is to ensure compatibility between nonpolar polyolefin matrices and CNTs, since the components have low interaction energy.[7,8] This is necessary for creating strong interface between filler particles and the polymer phase, thus providing efficient load transfer from matrix to nanotubes and, correspondingly, efficient reinforcement of composites. The problem is critical to polyolefins, while in the case of polar matrices, it has substantially easier solutions; thus, Zhang et al.[9,10] achieved high adhesion and strong interface between nylon-6 and moderately oxidized multiwall carbon nanotubes (MWCNTs) in nanocomposites prepared by simple melt compounding. Good filler−matrix compatibility provided enhanced MWCNT dispersion and resulted in considerable strengthening of composites and great mechanical performance. But using the same experimental approach, Tang et al.[11] and Bhattacharyya et al.[12] could not achieve good CNT dispersion and apparently strong interface in polyolefin matrices (high density polyethylene and polypropylene) because of the low compatibility between nonpolar polymers and nanotubes that resulted in predominant CNT aggregation and minor effect of nanotube incorporation on mechanical properties of materials. Side-wall CNT functionalization with short alkyl chains is a promising strategy for enhancing compatibility between nanotubes and polyolefins, however this way leads to overall complication of nanocomposite preparation and increased expensiveness of materials that is not preferred in industry.

We consider in situ polymerization method as the most effective approach for the synthesis of polyolefin-based nanocomposites that is capable of solving both problems: CNT aggregation and polymer/nanotube compatibilization due to the

* Corresponding autor. E-mail: kovalchuk@chph.ras.ru.
† N.N. Semenov Institute of Chemical Physics of Russian Academy of Sciences.
‡ N.M. Emanuel Institute of Biochemical Physics of Russian Academy of Sciences.
§ N.S. Enikolopov Institute of Synthetic Polymer Materials of Russian Academy of Sciences.

10.1021/ma800297e CCC: $40.75
Published on Web 04/17/2008

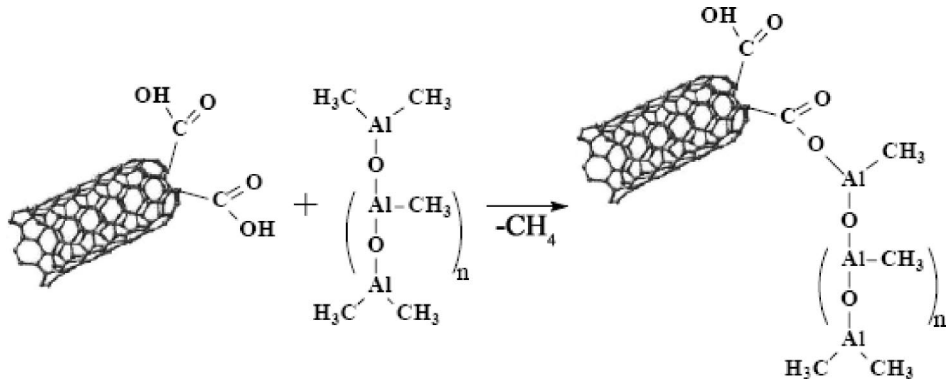

Figure 1. Scheme of chemical interaction between MAO and CNTs.

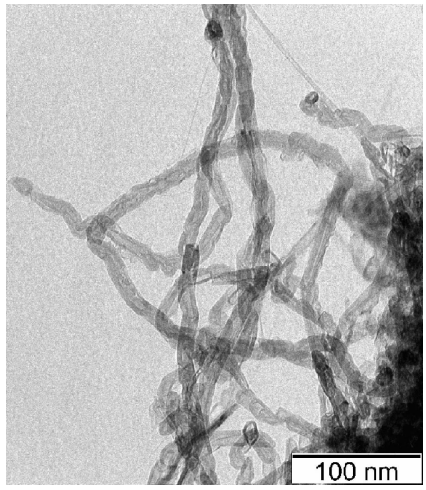

Figure 2. TEM micrograph of as-received MWCNTs.

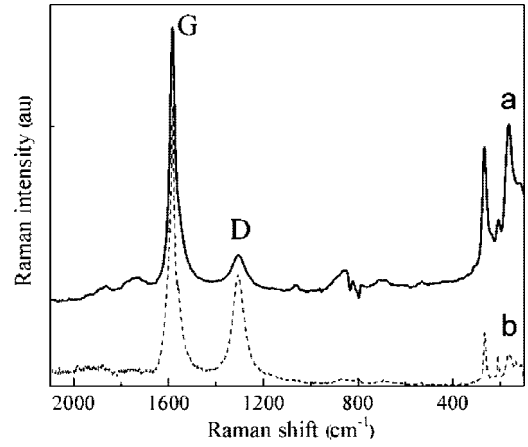

Figure 3. Raman spectra of acid treated (a) and of as-received MWCNTs (b). Spectra are normalized by G-line intensity and are offset along ordinate for clarity.

intimate contact between catalyst active sites and surface of filler particles.[13] This approach has been successfully applied for the incorporation of CNTs in various polymer matrices mostly via radical or polycondensation reaction routes,[14–17] but it has quite limited employment for the synthesis of polypropylene nanocomposites owing to its high complexity and sophistication, hindering the laboratory exploitation. Only few papers by the group of W. Kaminsky report about the use of in situ polymerization method for obtaining polypropylene/MWCNT nanocomposites,[6,13,18,19] and the corresponding data is obviously insufficient for the understanding of morphology and complex of nanocomposite properties.

In our work, we made a step forward toward the industrial realization of in situ polymerization approach for polypropylene/CNT nanocomposite synthesis and elaborated the new experimental technique that is quite feasible for industrial application, which has not been previously reported in literature. The distinct features of our method are following. (1) bulk of liquid propylene is used as a medium for CNT dispersion and subsequent polymerization reaction. Utilization of liquid monomer as a reaction medium allows obtaining of nanocomposites with high yields and high molecular weights (considering matrix polypropylene) and makes the synthesis easily scalable. (2) CNT dispersion via ultrasonication proceeds in the presence of the cocatalyst, methylaluminoxane (MAO). This leads to immobilization of MAO molecules on CNT surface by loose ionic interactions and, to a lesser extent, by virtue of covalent bonding (see scheme in Figure 1) to −COOH or −OH groups, which are inherent to partially oxidized CNTs. (3) The formation of catalytic active sites is accomplished by means of heterogenization of the metallocene catalyst precursor on CNT surface owing to chemical interaction of metallocene with MAO directly during the initial stage of polymerization at lowered temperature.

We assume that covalent bonding between MAO and CNTs has considerable impact on the morphology and properties of nanocomposites; MAO molecules chemically grafted to CNT surface form catalytic active species, yielding polypropylene chains attached directly to nanotubes. Though this labile linkage disrupts after quenching the polymerization reaction, it nevertheless provides intimate contact between polymer chains and filler particles contributing to matrix−filler compatibilization. In the present work, we use low-diameter MWCNTs, since they are regarded as the optimal reinforcement fibers for polymer composites.[20] Moreover, the lower the CNT diameter (and the higher surface area of the filler phase gained in prepolymerization suspension), the more efficient is the metallocene heterogenization on the nanotube surface achieved that leads to better CNT dispersion in nanocomposites.

In this paper, we report the synthesis and characterization of two series of CNT-filled nanocomposites based on principally different matrices: isotactic polypropylene (iPP), a high crystalline thermoplastic polymer, and stereoblock elastomeric polypropylene (elPP),[21] a nearly amorphous polymer with elastic behavior. Morphology of obtained nanocomposites and their thermal, mechanical, and electrical properties have been examined.

Experimental Section

Materials. Pristine CVD-grown MWCNTs (purity ≥95%, average diameter <10 nm, length range 5−15 μm) were purchased from Shenzhen Nanotech Port Co., China (trade name of product is L-MWNTs-10). As-received MWCNTs were purified and mildly oxidized by boiling in 30 wt % nitric acid for 1 h with subsequent

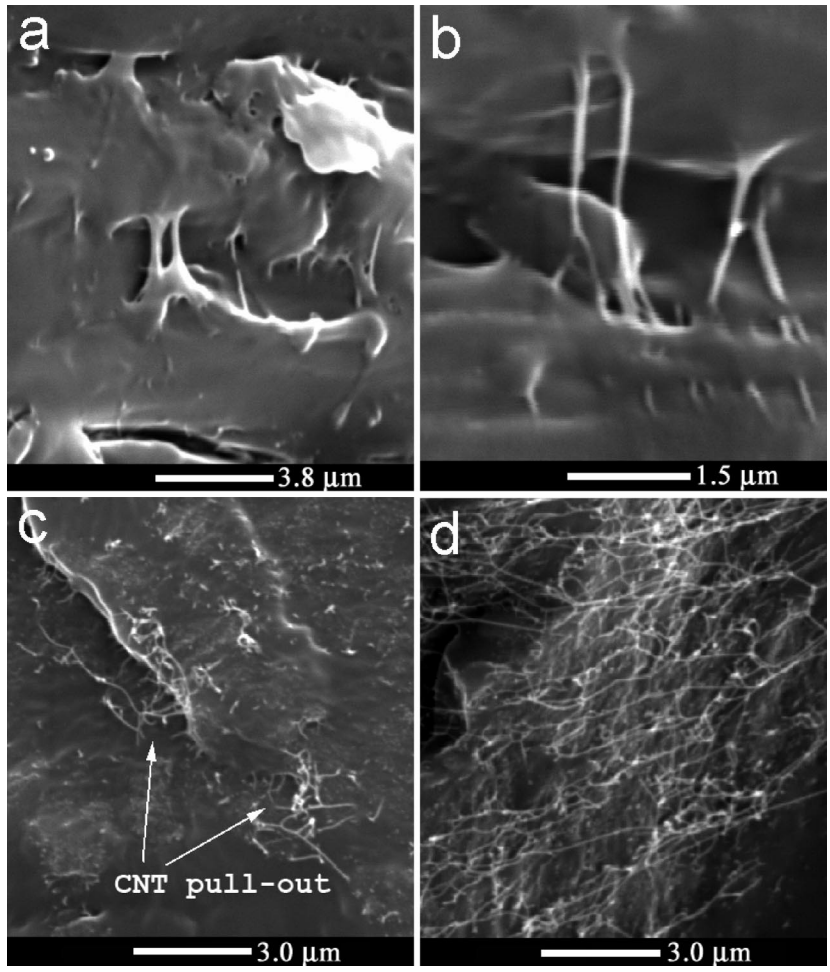

Figure 4. SEM images of the *i*PP/MWCNT nanocomposites: iPP/0.1 wt % MWCNT at low magnification (a) and at high magnification (b), iPP/0.4 wt % MWCNT (c), and iPP/2.1 wt % MWCNT (d).

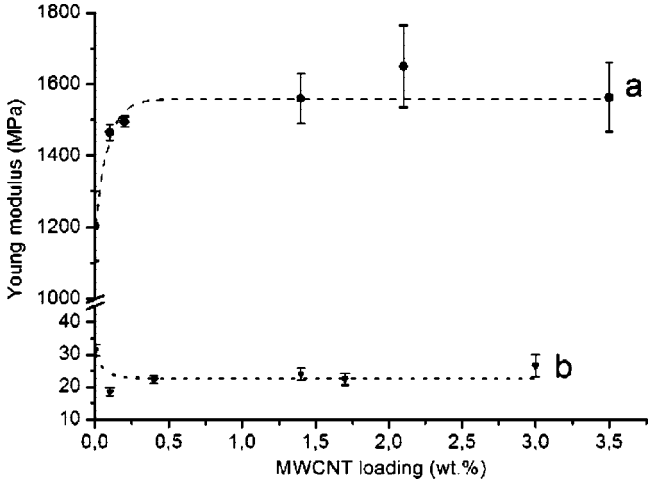

Figure 5. Young's modulus of iPP/MWCNT nanocomposites (a) and elPP/MWCNT nanocomposites (b) as a function of MWCNT loading.

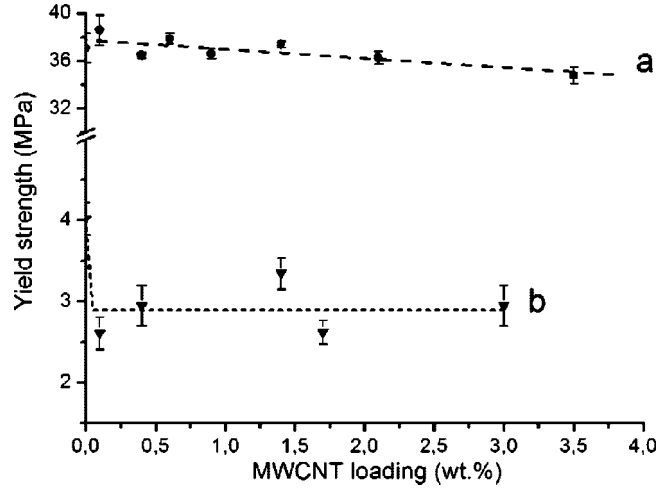

Figure 6. Correlations between yield strength and MWCNT content for iPP/MWCNT nanocomposites (a) and elPP/MWCNT nanocomposites (b).

settling at room temperature for 20 h. This procedure was carried out in order to remove the rest of amorphous carbon and impurities that might be poisonous for metallocene catalysts and to increase the content of carboxylic and hydroxyl groups on MWCNTs. The acid-treated MWCNTs were filtered and washed repeatedly with deionized water, dried in vacuum at 400 °C for 5 h, and then stored in argon atmosphere. Polymerization grade propylene was provided by Moscow Oil Refining Plant and used in nanocomposite synthesis without any additional treatment. Isospecific C_2-symmetry metallocene catalyst *rac*-$Me_2Si(2\text{-}Me\text{-}4\text{-}PhInd)_2ZrCl_2$ (MC-1) for iPP/MWCNT nanocomposite preparation was purchased from Boulder Scientific Co., and C_1-symmetry metallocene rac-[1-(9-η^5-Flu)-2-(5,6-cyclopenta-2-Me-1-η5-Ind)C_2H_4]-$ZrCl_2$ (MC-2) for obtaining elPP/MWCNT nanocomposites was synthesized in Moscow State University according to the technique reported earlier.[22] MAO as a 10 wt % solution in toluene was purchased from Witco. Metallocenes were used in the form of toluene solutions (0.01−0.03 wt %) preactivated with MAO.

Nanocomposite preparation. Polymerization experiments were carried out at 60 °C temperature and 2.5 MPa pressure in 200 cm^3

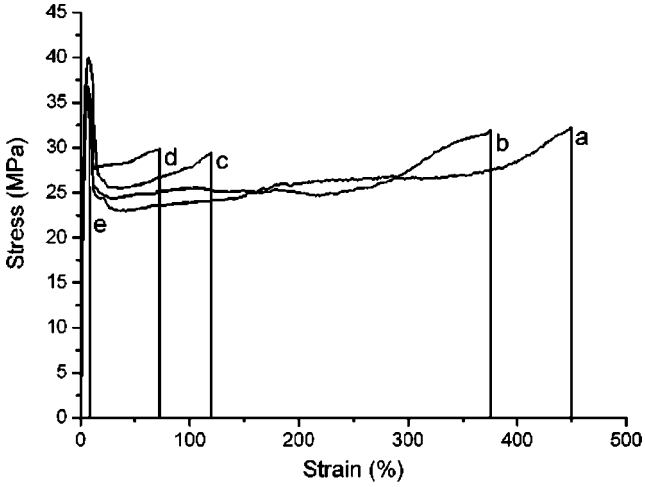

Figure 7. Tensile diagrams of iPP (a) and iPP/MWCNT nanocomposites containing 0.1 wt % MWCNT (b), 0.2 wt % MWCNT (c), 0.4 wt % MWCNT (d), and 2.1 wt % MWCNT (e).

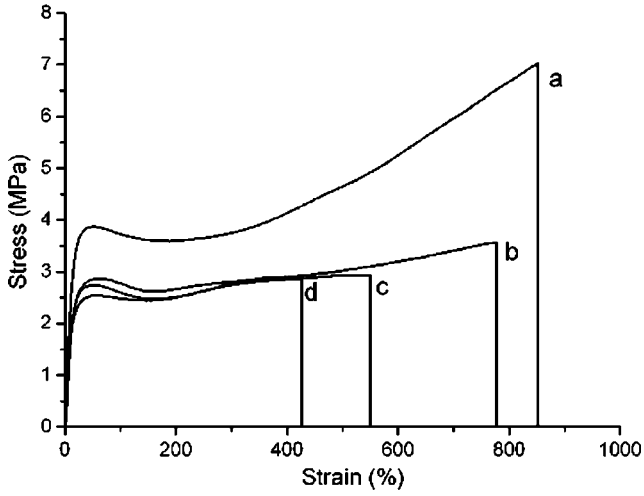

Figure 8. Tensile diagrams of elPP (a) and elPP/MWCNT nanocomposites containing 0.4 wt % MWCNT (b), 1.7 wt % MWCNT (c), and 3.0 wt % MWCNT (d).

stainless steel autoclave reactor equipped with an internal sonotrode for MWCNT ultrasonication and a high speed mechanical stirrer (3000 rpm). The reactor, containing the required amount of MWCNTs, was evacuated for 1.5 h at 60 °C before polymerization experiments and then filled with 150 mL of liquid propylene and 2.5−5 g of 10 wt % MAO solution. The prereaction mixture was sonicated then for 30 min with the use of 300W 40 kHz ultrasonic generator. Polymerization assisted by mechanical stirring was started immediately after MWCNT ultrasonication by injecting metallocene solution into the precooled (10 °C) reactor to provide homogeneous distribution of active sites on MWCNT surface. After a 2 min initial stage of polymerization, the reaction temperature was raised to 60 °C. Polymerizations were carried out for 10−15 min (for iPP nanocomposites) or 30−40 min (for elPP nanocomposites) and then quenched by adding ethanol. This noninterruptable sonication−polymerization procedure sequence allows efficient "catching" of nanotubes by polypropylene shell in the highly dispersed state without any sedimentation. After polymerization, the nanocomposite powder was extracted from the reaction mixture by simply depressurizing the unreacted propylene gas from the reactor.

Composition of the nanocomposites was controlled by adjusting three variables, namely, MWCNT weight, polymerization time, and metallocene amount. Catalyst amounts ranged between 3×10^{-7} and 5×10^{-7} mol for MC-1 and between 1×10^{-6} and 1.2×10^{-6} mol for MC-2. The MAO/zirconium molar ratio was kept within the bounds of 12000−14000 for MC-1/MAO catalyst system and 5000−7000 for MC-2/MAO.

After quenching the polymerization, the nanocomposites were placed for 24 h in ethanol acidified by hydrochloric acid in order to remove aluminum hydroxide and catalyst residues. After that, the materials were repeatedly washed with distilled water and ethanol and then dried in vacuum at 40 °C.

Characterization. Transmission electron microscopy (TEM) observations of MWCNT samples were performed on a LEO-912AB transmission electron microscope. Raman spectra of MWCNTs and the corresponding composites were acquired with the aid of Senterra Raman microscope (Bruker) furnished with a 785 nm laser excitation.

Molecular weights and molecular weight distributions of neat polymers were evaluated by GPC in a Waters 150C at 130 °C by using linear μ-styragel HT columns and 1,2,4-trichlorobenzene as the eluent. The molecular weights were determined by employing polystyrene calibration curve as a reference.

The uniaxial tensile testing of nanocomposites was performed at room temperature (20 °C) on an Instron 1122 machine at 50 mm/min tensile speed for iPP/MWCNT and 500 mm/min for elPP/MWCNT composites. The film samples for mechanical testing were prepared by hot pressing of nanocomposites at 190 °C and 10 MPa for 5 min and subsequent cooling at 16 K/min rate, and dog-bone specimens (with dimensions $35 \times 5 \times 0.5$ mm for iPP/MWCNT and $35 \times 5 \times 1$ mm for elPP/MWCNT series) were cut from films. Five specimens of each material were tested for reproducibility.

The morphology of fracture surfaces of the nanocomposite films was observed using a Hitachi S-520 scanning electron microscope (SEM). Isotropic film samples prepared as mentioned above were fractured in liquid nitrogen and gold-sputtered prior to SEM imaging.

DSC measurements were carried out on a Perkin-Elmer DSC-7 differential scanning calorimeter at 10 K/min scanning rate. After the first heating run, the samples were cooled down immediately and then heated again at the same rate (10 K/min). Results of the first cooling and of the second heating runs were taken into account. Thermogravimetry analysis (TGA) of nanocomposites was performed on a Perkin-Elmer TGA-7 instrument in argon atmosphere at 20 K/min heating rate.

DC conductivity of the materials was measured by utilizing a two-probe method at room temperature. Electrical properties of polypropylene/MWCNT nanocomposites in the microwave range (3.2−40 GHz) were evaluated by the cavity resonance method using KSVN R-2 instruments (Russia) with rectangular-shaped resonators (H_{0ln} operating mode). The cavity resonance method is based on the determination of resonance frequency change Δf and the change of cavity Q-factor ($1/Q - 1/Q_0$) when the measured sample is inserted into the cavity. Direct measurements yield real (ε') and imaginary (ε'') parts of the nanocomposite permittivity. The following equations were used for the estimation of permittivity and dielectric losses: $\varepsilon' - 1 = \Delta f\, V/f\, 2V_0$; $\varepsilon'' = [1/Q - 1/Q_0]V/4V_0$, where V is volume of the sample and V_0 is the cavity volume. Conductivity was extracted from the dielectric loss data using equation: $\varepsilon'' = i\kappa\lambda\sigma$, where $\kappa = 1/(2\pi c\varepsilon_0)$, λ is the wavelength, c is the velocity of light in vacuum, and ε_0 is the permittivity of vacuum.

Results and discussion

Characterization of MWCNTs and Effect of Chemical Treatment. Typical TEM image of as-received MWCNTs is shown in Figure 2 and represents the highly entangled morphology of CVD-grown nanotubes with average diameter around 10 nm. Surprisingly, noticeable amount of single wall carbon nanotubes was detected in the bulk of MWCNTs. Comparison of TEM images of pristine MWCNTs with purified and ultrasonicated MWCNTs (identical to those used in the nanocomposite syntheses) did not show evident nanotube shortening. Raman spectra of the acid-treated MWCNTs reveal noticeable decrease of amorphous carbon content; this follows from the reduction of disorder mode band intensity (D peak in Figure 3).

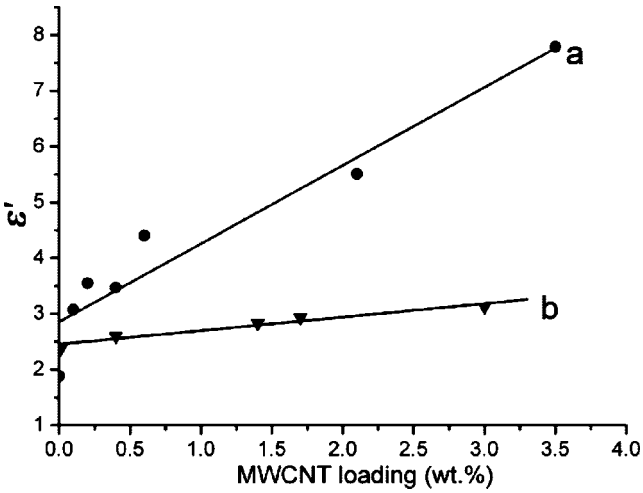

Figure 9. Permittivity at frequency 4.8 GHz as a function of filler loading for iPP/MWCNT nanocomposites (a) and elPP/MWCNT nanocomposites (b).

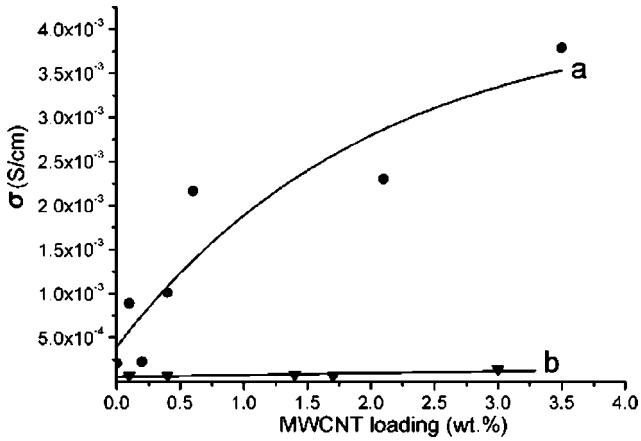

Figure 10. Electrical conductivity at frequency 4.8 GHz as a function of filler loading for iPP/MWCNT nanocomposites (a) and elPP/MWCNT nanocomposites (b).

Nanocomposite synthesis results. The iPP/MWCNT nanocomposites with filler loadings from 0.1 to 3.5 wt % and elPP/MWCNT nanocomposites containing 0.1−3.0 wt % MWCNTs were obtained by in situ polymerization method in liquid propylene medium. Molecular weights of the neat polymers synthesized under identical conditions to the nanocomposites are $M_w \sim 600\,000$ ($M_w/M_n = 2.2$) for iPP and $M_w \sim 63\,000$ ($M_w/M_n = 2.1$) for elPP. Catalyst activity remains unchanged in presence of MWCNTs either for MC-1/MAO (~100 kg iPP/(mmol Zr h)) or for MC-2/MAO (~20 kg elPP/(mmol Zr h)). Marked differences in nanocomposite morphology between iPP- and elPP-based composites must be taken into account because of the fact that iPP is insoluble in liquid propylene at 60 °C and firmly covers CNT surface, while elPP is easily soluble, and thus phase separation and nanotube sedimentation during polymerization should be expected in this case. Hence, we can classify our elPP/MWCNT nanocomposite preparation method as a combination of in situ polymerization and solution blending technique, yet iPP/MWCNT nanocomposites are obtained by true in situ polymerization.

Microstructure of the Nanocomposites. Scanning electron microscopy imaging (Figure 4) of iPP/MWCNT nanocomposites reveals homogeneous distribution of filler particles within polymer matrix. Intense ultrasonication results in effective MWCNT dispersion and successfully prevents nanotube agglomeration, so well-separated individual CNTs prevail in filler phase. Noticeable differences in fracture morphology of nanocomposites depending on MWCNT loading are observed. Thus, the low nanotube loading (0.1 wt %) sample demonstrates the most efficient polymer reinforcement; CNTs appear broken upon nanocomposite fracturing (Figure 4a) that indicates effective load transfer from matrix to nanotubes. On the magnified image of the sample's fracture surface (Figure 4b), we see nanotubes bridging two polymer lumps; MWCNTs are perfectly covered with polypropylene shell and strongly embedded in the matrix that displays perfect interfacial adhesion. On increasing the filler content (Figure 4c), we observe the nanotubes both are partly broken and partly demonstrate the tendency to pull out of matrix. This CNTs pulling out evidence the decrease of interfacial adhesion in the material as compared to the first nanocomposite sample. Nanotube pull-out becomes predominant at high filler loadings (Figure 4d) that signify considerable deterioration of CNT reinforcement efficiency in composite. This fracture behavior clearly correlates with the mechanical properties of nanocomposites and will be discussed below.

Mechanical Properties of the Nanocomposites. Two diverse patterns in nanocomposite mechanical behavior are observed corresponding to different matrices. MWCNT incorporation has considerable impact on iPP tensile properties; noticeable Young's modulus increase by ~22% from ~1200 to ~1465 MPa takes place only at 0.1 wt % filler loading, and further modulus enhancement continues up to 3.5 wt % MWCNT loading (Figure 5, a). Ultimate Young's modulus improvement of iPP is ~37% (from ~1200 to ~1650 MPa) at 2.1 wt % MWCNT content. Subsequent moderate modulus drop at a loading of 3.5 wt % of MWCNTs is apparently connected with the nanotube agglomeration that is inevitable at such a high CNT concentrations. Yield strength of iPP-based nanocomposites has relatively minor effect corresponding to the nanotube loading and shows a decreasing trend (Figure 6, a). This yielding behavior indicates that more efficient polymer reinforcement is achieved at low MWCNT concentrations (0.1−0.6 wt %), whereas dewetting effect becomes more pronounced at higher loadings that is in agreement with SEM data (nanotube pull-out signifies dewetting). This lowering of interfacial adhesion could be related to the regular increase in direct contacts between individual nanotubes at higher MWCNT loadings (that is especially relevant to CVD-grown CNTs which typically form highly entangled networks) that would reduce matrix−nanotube contact area per single MWCNT. Anyway, the achieved interfacial interaction between iPP and MWCNTs is insufficient for substantial polymer reinforcement and is the subject for improvement by nanotube functionalization.

Unlike iPP-based nanocomposites, filling of elPP with MWCNTs is totally detrimental to materials' properties. Thus, the marked decrease in composite Young's modulus (Figure 5, b) is obviously connected with the nanotube agglomeration and improper filler distribution that arises from the synthesis peculiarities. Polymer yield strength also decreases with MWCNT loading, which means total incompatibility between elPP and nanotubes. This incompatibility could be related to the low molecular weight of elPP, since low molecular weight polymers are regarded to have weak interaction with nanotubes.[23]

Tensile diagrams of iPP/MWCNT nanocomposites are presented in Figure 7. They show strong MWCNT influence on polypropylene chain flexibility causing severe matrix embrittlement. Apparently, nanotubes which form entangled networks are integrated into polypropylene crystalline phase and act as obstacles to lamellae stretching. This embrittlement effect considerably descends for the semiamorphous elPP (Figure 8). We see that even high MWCNT loading (3 wt %) does not provoke noticeable decrease of elPP ultimate strain, while only 0.2 wt % filler concentration is sufficient to reduce iPP tensile strain by 4-fold. This sharp transition in iPP tensile behavior

Table 1. Melting Temperatures, Fusion Enthalpies, Crystallization Temperatures, and Crystallinity Degrees of iPP/MWCNT nanocomposites

Material	T_m (°C)	ΔH_m (J/g)	T_c (°C)	X_c[a] (%)
iPP	156.6	90.7	108.9	43.3
iPP/0.1 wt % MWCNT	156.3	97.2	112.7	46.5
iPP/0.4 wt % MWCNT	157.1	92.2	117.1	44.1
iPP/0.6 wt % MWCNT	157.6	97.3	115.6	46.5
iPP/0.9 wt % MWCNT	158.5	95.8	116.2	45.8
iPP/1.4 wt % MWCNT	158.1	93.7	122.5	44.8
iPP/2.1 wt % MWCNT	157.6	93.4	121.0	44.6
iPP/3.5 wt % MWCNT	157.5	94.8	122.7	45.3

[a] Determined using the following expression: $X_c = \Delta H_m \Delta H_m^0 \times 100$, where $\Delta H_m^0 = 209$ J/g is the theoretical enthalpy value for a 100% crystalline iPP.[30]

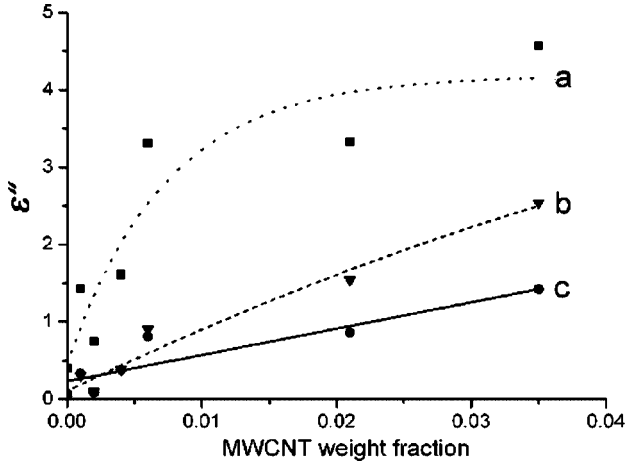

Figure 11. Correlation between dielectric losses and nanotube loading for iPP/MWCNT nanocomposites at frequencies 3.2 GHz (a), 11 GHz (b), and 4.8 GHz (c).

from plastic to brittle mechanism is another evidence for the low interaction between polymer chains and MWCNTs. It should be noted that the ultimate tensile strength of iPP/MWCNT nanocomposites is nearly independent of nanotube content and remains at 30 ± 1 MPa that also certifies efficient CNT distribution in matrix, while the evident decrease of this parameter for elPP/MWCNT materials (Figure 8) suggests strong influence of nanotube agglomeration in the latter system.

Electrical Properties. DC conductivity measurements of iPP/MWCNT and elPP/MWCNT nanocomposites show no percolation behavior within the employed range of nanotube loadings (up to 3.5 wt %). Electrical resistivity of all materials exceeds 1×10^{15} Ohm cm, the instrument's sensitivity threshold. It is in agreement with the literature data for polyethylene/MWCNT nanocomposites.[24] Obviously, the absence of percolation transition is due to the lack of conductive paths in materials. It can be explained by the predominant exfoliation of nanotube aggregates followed by perfect coating of CNTs with the polymer and the homogeneous filler distribution achieved via our in situ polymerization method in the case of iPP/MWCNT nanocomposites, but the above reason for the response in elPP/MWCNT materials is still debatable. Since CNT aggregation is considered as a critical factor for nanocomposite electrical conductivity,[25] improved electrical properties of elPP/MWCNT composites in comparison with iPP/MWCNT are expected. Nevertheless, the resultant conductivity of elPP/MWCNT is of the same level as that of iPP/MWCNT, and further detailed investigation will be required in order to explain this fact.

Microwave experiments demonstrate marked differences in electrical properties of iPP/MWCNT nanocomposites as compared to elPP/MWCNT nanocomposites. A rapid growth of permittivity with increasing nanotube content is observed for iPP/MWCNT nanocomposites unlike elPP/MWCNT composites (Figure 9). The slow increase of elPP/MWCNT permittivity can be attributed to nanotube agglomeration, which will be discussed in detail below. Even greater difference of the same origin is observed for electrical conductivity values of iPP/MWCNT and elPP/MWCNT nanocomposites (Figure 10); the conductivity of iPP/MWCNT materials is approximately 1 order of magnitude higher in comparison with elPP/MWCNT. This behavior corresponds to different frequencies in the microwave range.

As mentioned above, we attribute low permittivity and conductivity values of elPP/MWCNT nanocomposites to nanotube agglomeration. In order to prove it, we carried out the following calculations. The slope of the line representing permittivity vs filler fraction correlation (Figure 9) depends on the filler particles depolarization coefficient, which is determined by the aspect ratio of filler particles (length/diameter ratio for nanotubes). Analysis of these functional dependences has been performed with the use of the theoretical model described in literature.[26]

Electrical properties of polymer composite systems containing spherical filler particles are adequately described by Bruggeman's equation up to 30 vol % filler concentration:[27]

$$\frac{\varepsilon_f - \varepsilon}{\varepsilon_f - \varepsilon_m}\left(\frac{\varepsilon_m}{\varepsilon}\right)^{1/3} = 1 - v_f \tag{1}$$

Bruggeman's equation can be generalized for ellipsoidal filler shape:[28]

$$\frac{\varepsilon_f - \varepsilon}{\varepsilon_f - \varepsilon_m}\left(\frac{\varepsilon_m}{\varepsilon}\right)^{\alpha}\left(\frac{\varepsilon_f\beta + \varepsilon_m}{\varepsilon_f\beta + \varepsilon}\right)^{\gamma} = 1 - v_f \tag{2}$$

where $\alpha = 3A(1 - 2A)/(2 - 3A)$, $\beta = (2 - 3A)/(1 + A)$, $\gamma = 2(3A - 1)/(1 + 3A)/(2 - 3A)$, and $A = A_y = A_z$ is the depolarization coefficient.

The following equations were used to derive the functions $\varepsilon'(v_f)$ and $\varepsilon''(v_f)$, suitable for the description of composites containing elongated filler particles (i.e., nanotubes):[28]

$$\varepsilon = \varepsilon_m + \frac{v_f}{3}\sum_1^3 \frac{\varepsilon_f - \varepsilon_m}{1 + A_i(\varepsilon_f/\varepsilon_m - 1)} \tag{3}$$

$$\varepsilon = \varepsilon_m + \frac{v_f}{3(1 - v_f)}\sum_1^3 \frac{\varepsilon_f - \varepsilon_m}{1 + A_i(\varepsilon_f/\varepsilon_m - 1)} \tag{4}$$

where ε is the complex dielectric constant and A_i are the depolarization coefficients. Depolarization coefficients for the prolate ($l > d$) ellipsoids in uniform electric field were taken from:[29]

$$A_x = \frac{1 - e^2}{e^3}(arth(e) - e),\ A_y = A_z = (1 - A_x)/2,\ e = \sqrt{1 - d^2/l^2} \tag{5}$$

Dielectric losses of filler was taken in the following form:

$$\varepsilon'' = i\kappa\lambda\sigma \tag{6}$$

where $\kappa = 1/(2\pi c\varepsilon_0)$, σ is the conductivity of fibers, λ is the wavelength, and ε_0 is the vacuum permittivity.

The following minor parameters were used: $\nu = \varepsilon_m/\varepsilon_f \ll 1$ and $\mu = d/l \ll 1$ (conductivity of the matrix is negligible compared to that of filler). It follows from eq 5 that if $\mu \ll 1$ then $A_x \ll 1$ is also a minor parameter. Equations 3 and 4 were

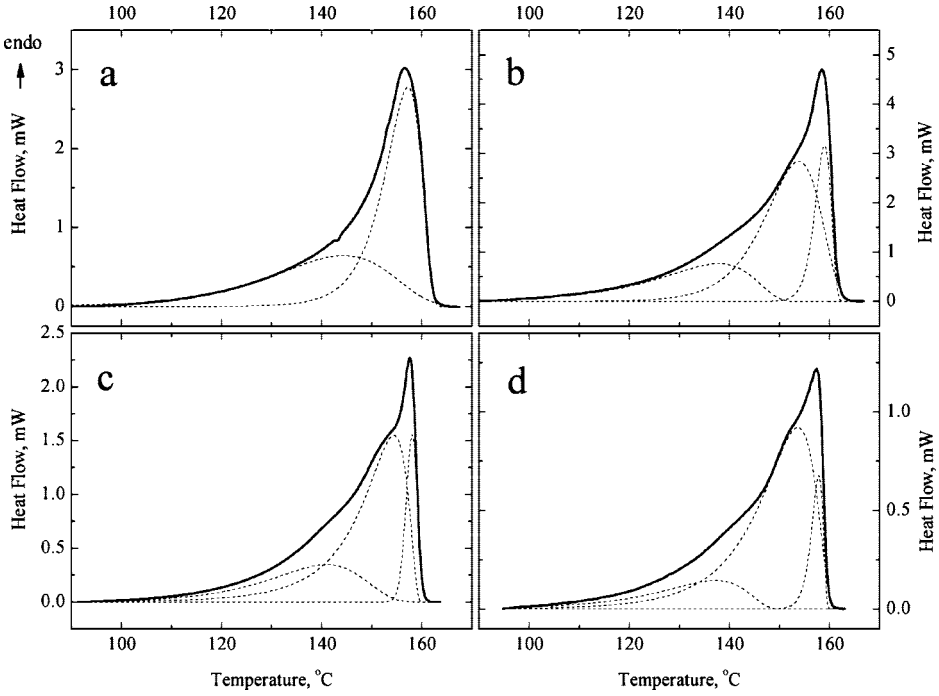

Figure 12. 2nd melting DSC thermograms for the iPP/MWCNT nanocomposites illustrating variability of the polypropylene crystal phase compositions depending on the MWCNT content: (a) neat iPP, (b) 0.9 wt % MWCNT, (c) 2.1 wt % MWCNT, and (d) 3.5 wt % MWCNT.

expanded over parameters ν and A_x and, using eqs 5 and 6, the following expressions were derived:

$$\varepsilon = \varepsilon_m + \frac{v_f \varepsilon_m / 3A_x}{1 - i\varepsilon_m / \kappa\lambda\sigma A_x} \tag{7}$$

$$\varepsilon = \varepsilon_m + \frac{v_f}{1 - v_f} \frac{v_f \varepsilon_m / 3A_x}{1 - i\varepsilon_m / \kappa\lambda\sigma A_x} \tag{8}$$

Separating real and imaginary parts of eq (8), one can write:

$$\varepsilon' = \varepsilon_m + \frac{v_f}{1 - v_f} \frac{\varepsilon_m / 3A_x}{1 + (\varepsilon_m / k\lambda\sigma A_x)^2} \tag{9}$$

$$\varepsilon'' = \frac{v_f}{1 - v_f} \frac{\varepsilon^2 / 3k\lambda\sigma A_x^{\,2}}{1 + (\varepsilon_m / k\lambda\sigma A_x)^2} \tag{10}$$

Equation 9 was fitted to the experimental data with A_x as a parameter. Then, eq 5 was used to estimate the relative filler aspect ratios for iPP/MWCNT and elPP/MWCNT systems. As a result, the approximate nanotube aspect ratio for iPP/MWCNT nanocomposites is ~25, and for elPP/MWCNT, it is ~2. These values obtained from microwave electrical measurements only roughly correspond to the actual CNT aspect ratios in the synthesized materials and can be used only for the relative comparison of nanotube aspect ratios for the two systems. Thus, we can make a conclusion that the spheroidal MWCNT clusters formed in elPP/MWCNT nanocomposites are ~12 times higher in diameter compared to those formed in iPP/MWCNT nanocomposites.

Dielectric loss data for iPP/MWCNT nanocomposites at different frequencies are presented in Figure 11. High dielectric losses in the microwave range for the obtained composites indicate substantial energy dissipation within materials. Relatively low permittivity values and considerable dielectric losses infer that the synthesized nanocomposites can find use as efficient electromagnetic shielding materials and microwave absorbing filters.

Thermal properties. Thermal characteristics of iPP/MWCNT nanocomposites are summarized in Table 1. The incorporation of MWCNTs in iPP matrix has moderate impact on the fusion enthalpy (ΔH_m) of the polymer; we observe certain growth of this parameter that indicates slight increase of the polymer crystallinity, but there is no definite correlation between CNT loading and iPP crystallinity degree (X_c). The widening of the iPP melting peak (Figure 12) with the increase of the MWCNT loading evidence the formation of imperfect polymer crystallites and the broadening of crystallite size distribution. By applying Fraser−Suzuki peak separation method to the melting thermograms, we demonstrate that variability of iPP crystal phase compositions takes place upon nanotube incorporation and contribution of the most thermodynamically stable phase dramatically decreases. Carbon nanotubes exert evident influence as nucleating agents causing the rise of polypropylene crystallization temperature (T_c), Figure 13. This improvement in crystallization behavior is favorable for the processing of the respective materials.

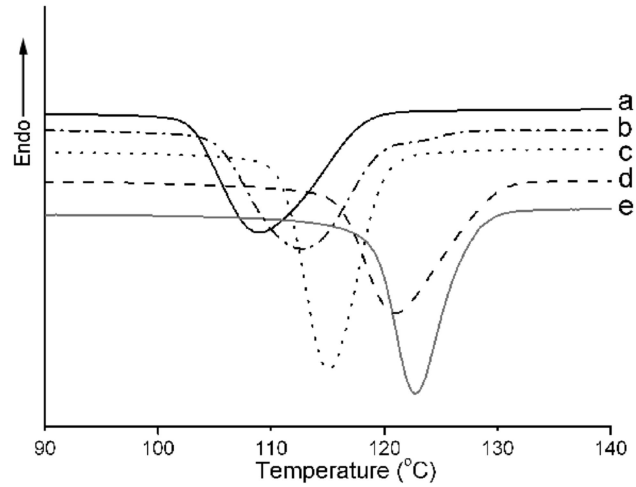

Figure 13. Crystallization DSC thermograms of iPP (a) and iPP/MWCNT nanocomposites containing 0.1 wt % MWCNT (b), 0.2 wt % MWCNT (c), 2.1 wt % MWCNT (d), and 3.5 wt % (e).

Thermal Degradation of Nanocomposites. Thermal degradation behavior of iPP/MWCNT nanocomposites has been investigated by employing TGA analysis in inert argon atmosphere. TGA profiles of nanocomposites are presented in Figure 14. We

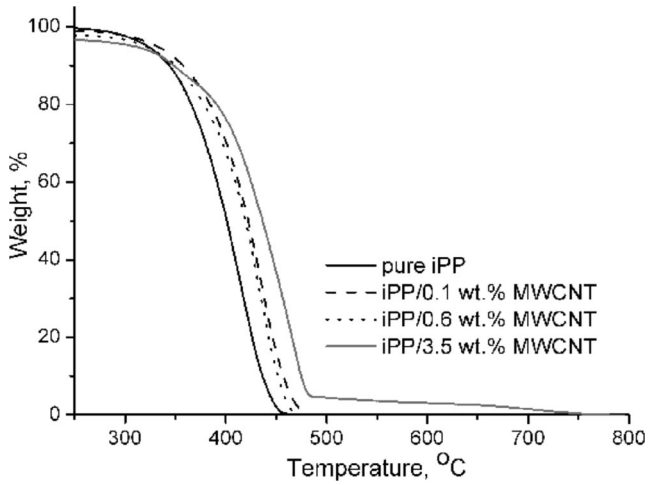

Figure 14. TGA profiles of iPP/MWCNT nanocomposites.

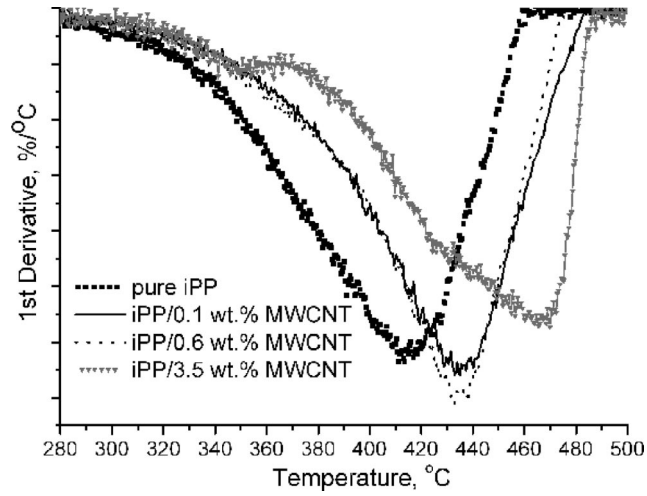

Figure 15. 1st Derivative curves corresponding to the TGA profiles of iPP/MWCNT nanocomposites.

see that even quite negligible amounts of filler nanoparticles contribute considerably to the rise of thermal degradation temperature; the addition of 0.1 wt % MWCNTs increases the temperature of maximum weight loss (peak temperature on first derivative curve, Figure 15) of the nanocomposite by ~30 °C in comparison with pristine polypropylene, and this parameter shifts higher with further increase in the filler content. An outstanding increase in thermal stability has been achieved by just introducing 3.5 wt % of MWCNTs; at this loading, the maximum weight loss temperature of the nanocomposite surpasses the characteristic of the neat polymer by ~60 °C. This thermal stabilization effect is mostly connected with the formation and stabilization of CNT-bonded macroradicals[31] and nanotube barrier effect, implying hindered transport of polymer decomposition products within a volume of the composite.[32]

Conclusion

The reported in situ polymerization method shows great potential in terms of effectively dispersing CNTs in polypropylene and, thus, development of advanced polymer nanocomposites. The entire range of iPP properties is considerably modified even at low MWCNT loadings (up to 1 wt %). Though very efficient distribution of MWCNTs in iPP matrix has been achieved, additional efforts are needed to provide high interfacial adhesion and enhanced polymer reinforcement. We expect that the improvement of polypropylene−nanotube compatibility and load transfer from matrix to nanotubes can be realized via CNT sidewall functionalization with alkyl chains. Our further investigation will be focused on this modification.

Acknowledgment. Authors gratefully thank Dr. Anastasia V. Bolshakova and Dr. Sergey S. Abramchuk from Moscow State University for the assistance in electron microscopy observations. This work was supported by Haldor Topsoe A/S grant.

References and Notes

(1) Iijima, S. *Nature* **1991**, *354*, 56.
(2) Ajayan, P. M.; Suhr, J.; Koratkar, N. *J. Mater. Sci.* **2006**, *41*, 7824.
(3) Ajayan, P. M. *Chem. Rev.* **1999**, *99*, 1796.
(4) Ajayan, P. M.; Tour, J. M. *Nature* **2007**, *447*, 1067.
(5) Moniruzzaman, M.; Winey, K. I. *Macromolecules* **2006**, *39*, 5194–5205.
(6) Wiemann, K.; Kaminsky, W.; Gojny, F. H.; Schulte, K. *Macromol. Chem. Phys.* **2005**, *206*, 1472–1478.
(7) Zheng, Q.; Xue, Q.; Yan, K.; Hao, L.; Li, Q.; Gao, X. *J. Phys. Chem. C* **2007**, *111*, 4628–4635.
(8) McIntosh, D.; Khabashesku, V. N.; Barrera, E. V. *Chem. Mater.* **2006**, *18*, 4561–4569.
(9) Zhang, W. D.; Shen, L.; Phang, I. Y.; Liu, T. *Macromolecules* **2004**, *37*, 256–259.
(10) Liu, T.; Phang, I. Y.; Shen, L.; Chow, S. Y.; Zhang, W.-D. *Macromolecules* **2004**, *37*, 7214–7222.
(11) Tang, W.; Santare, M. H.; Advani, S. G. *Carbon* **2003**, *41*, 2779–2785.
(12) Bhattacharyya, A. R.; Sreekumar, T. V.; Liu, T; Kumar, S.; Ericson, L. M.; Hauge, R. H.; Smalley, R. E. *Polymer* **2003**, *44*, 2373–2377.
(13) Kaminsky, W.; Wiemann, K. *Composite Interfaces* **2006**, *13* (4−6), 365–375.
(14) Kumar, S.; et al. *Macromolecules* **2002**, *35*, 9039–9043.
(15) Velasco-Santos, C.; et al. *Chem. Mater.* **2003**, *15*, 4470–4475.
(16) Moniruzzaman, M.; Chattopadhyay, J.; Billups, W. E.; Winey, K. I. *Nano Lett.* **2007**, *7* (5), 1178–1185.
(17) Kim, S. T.; Choi, H. J.; Hong, S. M. *Colloid Polym. Sci.* **2007**, *285*, 593–598.
(18) Kaminsky, W.; Funck, A.; Wiemann, K. *Macromol. Symp.* **2006**, *239*, 1–6.
(19) Funck, A.; Kaminsky, W. *Compos. Sci. Technol.* **2007**, *67* (5), 906–915.
(20) Cadek, M.; Coleman, J. N.; Ryan, K. P.; Nicolosi, V.; Bister, G.; Fonseca, A.; Nagy, J. B.; Szostak, K.; Beguin, F.; Blau, W. J *Nano Lett.* **2004**, *4* (2), 353–356.
(21) Dietrich, U.; Hackmann, M.; Rieger, B.; Klinga, M.; Leskela, M. *J. Am. Chem. Soc.* **1999**, *121*, 4348.
(22) Nedorezova, P. M. *Russ. Chem. Bull., Int. Ed.* **2005**, *54* (2), 400–413.
(23) Mu, M.; Winey, K. I. *J. Phys. Chem. C* **2007**, *111*, 17923–17927.
(24) McNally, T.; Potschke, P.; Halley, P.; Murphy, M.; Martin, D.; Bell, S. E. J.; Brennan, G. P.; Bein, D.; Lemoine, P.; Quinn, J. P *Polymer* **2005**, *46*, 8222–8232.
(25) Sandler, J. K. W.; Kirk, J. E.; Kinloch, I. A.; Shaffer, M. S. P.; Windle, A. H. *Polymer* **2003**, *44*, 5893–5899.
(26) Ponomarenko, A.; Shevchenko, V.; Figovsky, O. L. *Sci. Isr.−Technol. Advantages* **2005**, *7*, 37–52.
(27) Scarisbrick, R. M. *J. Phys. D: Appl. Phys.* **1973**, *6*, 2098–3009.
(28) Reynolds, J. A.; Hough, J. M. *Proc. Phys. Soc.* **1957**, *70* (8,425B), 769–775.
(29) Landau, L. D.; Lifshitz, E. M.; Pitaevskii, L. P. In *Electrodynamics of Continuous Media (Course of Theoretical Physics)*, 2nd ed.; Elsevier Butterworth-Heinemann: Oxford, 1984; Vol. *8.*
(30) Wunderlich, B. In *Macromolecular Physics*; Academic Press: New York, 1976; Vol. *II.*
(31) Raravikar, N. R.; Schadler, L. S.; Vijayaraghavan, A.; Zhao, Y.; Wei, B.; Ajayan, P. M. *Chem. Mater.* **2005**, *17*, 974–983.
(32) Marosfoi, B. B.; Szabo, A.; Marosi, Gy.; Tabuani, D.; Camino, G.; Pagliari, S. *J. Therm. Anal. Calorim.* **2006**, *86* (3), 669–673.

MA800297E